http://www.pjbs.org

PJBS

ISSN 1028-8880

Pakistan Journal of Biological Sciences

ANSInet
Asian Network for Scientific Information
308 Lasani Town, Sargodha Road, Faisalabad - Pakistan

OPEN ACCESS Pakistan Journal of Biological Sciences

ISSN 1028-8880
DOI: 10.3923/pjbs.2026.76.91

Research Article
Gynura procumbens Modulates VEGF Expression in Diabetic Wounds: Evidence from Immunohistochemistry and *in silico* Analysis

[1]Risma Dumiri Manurung, [1]Suriani Ginting, [2]Syahputra Wibowo, [3]Naufal Abiyyu, [4]Alfia Fitrianita and [5]Putri Cahaya Situmorang

[1]Department of Nursing, Politeknik Kesehatan Kementerian Kesehatan Medan, Indonesia
[2]Eijkman Research Center for Molecular Biology, National Research and Innovation Agency, 16911, Bogor, Indonesia
[3]Department of Biochemistry, Faculty of Mathematic and Natural Science, IPB University, Bogor, Indonesia
[4]Department of Biotechnology, Graduate School, IPB University, Bogor, Indonesia
[5]Department of Biology, Faculty of Mathematics and Natural Sciences, Universitas Sumatera Utara, Medan, Indonesia

Abstract

Background and Objective: Chronic hyperglycemia causes oxidative stress, immunological dysfunction and decreased angiogenesis, compromising wound healing. Wound healing requires VEGF, which stimulates angiogenesis and tissue regeneration. The aim of this study was to assess the effect of the ethanolic extract of *Gynura procumbens* leaves on VEGF expression in diabetic wound tissue using *in vivo* and *in silico* approaches. **Materials and Methods:** This study divided 30 alloxan-induced rats into five groups: Diabetic controls and those given Bioplacenton ointment and topical *G. procumbens* extract at 100, 200 and 300 mg/kg bw. Histology included hematoxylin-eosin staining and VEGF immunohistochemistry. The active chemicals of *G. procumbens* were examined using LC-MS/MS and VEGF was tested *in silico* utilizing molecular docking and dynamics. Data were analyzed using Kruskal-Wallis and Mann-Whitney tests, with results expressed as Mean±SD and significance set at $p<0.05$. **Results:** *Gynura procumbens* extract increased epithelial thickness, collagen density and balanced the number of fibroblasts in diabetic wounds, with the best results at a dose of 300 mg/kg body weight. VEGF expression increased significantly in group A3 compared to the untreated diabetic group. *In silico* tests showed that Mahuannin F had the highest binding affinity for VEGF (-7.2 kcal/mol) and was able to stabilize the VEGF structure disrupted by alloxan through hydrogen and hydrophobic interactions. Molecular dynamics simulations supported the conformational stabilization of VEGF by Mahuannin F. **Conclusion:** Diabetes wounds with topically administered *G. procumbens* extract had higher VEGF expression and better skin tissue architecture. Active substances like Mahuannin F, VEGF structural stabilizers, promote this chemical process.

Key words: Diabetic wounds, *Gynura procumbens*, VEGF, Mahuannin F, molecular docking, hyperglycemia

Citation: Manurung, R.D., S. Ginting, S. Wibowo, N. Abiyyu and A. Fitrianita, 2026. *Gynura procumbens* modulates VEGF expression in diabetic wounds: evidence from immunohistochemistry and *In silico* analysis. Pak. J. Biol. Sci., 29: 76.91.

Corresponding Author: Putri Cahaya Situmorang, Department of Biology, Faculty of Mathematics and Natural Sciences, Universitas Sumatera Utara, Medan, Indonesia

Competing Interest: The authors have declared that no competing interest exists.

Data Availability: All relevant data are within the paper and its supporting information files.

INTRODUCTION

The process of wound healing is catabolic and necessitates increased nutritional consumption. Diabetes can impair the immune system, heightening vulnerability to infections and reducing the body's ability to combat pathogens[1]. An infected wound exhibits a significantly extended healing duration. In diabetes patients, wound healing is oriented towards catabolism due to reduced anabolic hormone levels and increased inflammatory cytokines, which worsen insulin resistance[2]. Careful management of blood glucose levels will improve wound healing outcomes in diabetic patients[1]. Increased oxygen levels, judicious antibiotic use and specific metabolic abnormalities can enhance burn recovery[3]. Diabetes is common in burn patients and can negatively impact results[4]. Increased blood glucose levels can alter blood chemistry, compromising the body's defenses and slowing the immune response[5]. Wound healing in individuals with diabetes is more complex than in those without the condition. The mechanisms of apoptosis in wounds are crucial for preserving tissue homeostasis. However, abnormal apoptosis triggers uncontrolled inflammation in wounds, hinders angiogenesis and prevents proper re-epithelialization[6]. Consequently, apoptosis profoundly influences the healing process of diabetic wounds. Cells lost from wounds may exit through one of three mechanisms: necrosis, emigration or apoptosis[6]. Recent studies demonstrate that apoptosis is the primary factor leading to decreased cellularity during various stages of healing[6].

Apoptosis or programmed cell death, is precisely regulated and distinguished by certain morphological and molecular characteristics. During wound healing, the modification of granulation tissue is associated with fibroblast death. The equilibrium between cell proliferation and death is a crucial determinant in cell population dynamics[7]. Inflammatory mediators and advanced glycation end products are more concentrated in diabetic wounds and they can activate apoptotic pathways, ROS production, caspase-9 and caspase-3 activation, the pro-apoptotic transcription factor FOXO1 and MAP kinase signaling pathways[8]. The FOXO1 regulates the production of pro-apoptotic genes, which trigger cell death; its exact mechanism of action depends on the specific cell or tissue type[9]. Vascular Endothelial Growth Factor (VEGF) functions as a mitogen for endothelial cells, a chemotactic factor and a promoter of vascular permeability[10]. The VEGF is notable for its influence on various aspects of the wound healing process, including angiogenesis, as well as, more recently, epithelialization and collagen deposition[10]. Considering that angiogenesis is crucial for wound healing, VEGF may be employed in patients with non-healing wounds in the future, either as a monotherapy or in combination[11]. Diabetes causes an increase in the number of apoptotic fibroblasts. The VEGF facilitates angiogenesis and influences wound closure, epidermal repair, granulation tissue formation and apoptosis regulation via the activation of the caspase family[12].

Gynura procumbens (Sambung Nyawa) is a native Indonesian plant utilized for its culinary purposes in salads and its medicinal properties in diabetes treatment[13,14]. The utilization of *Gynura procumbens* leaf extract as a natural remedy for type II diabetes has shown success, even when employing merely warm water[15,16]. *Gynura procumbens* is a notable traditional plant in Southeast Asia, extensively utilized for treating inflammation, renal pain, hypercholesterolemia, diabetes, neoplasia and hypertension[17-19]. This work sought to evaluate the effects of topical application of *Gynura procumbens* leaf extract on VEGF expression and skin tissue regeneration in a diabetic wound model through *in vivo* and *in silico* approaches. This study seeks to identify the principal phytoconstituents of *Gynura procumbens* ethanol extract that may operate as VEGF modulators and support molecular modeling. The idea posits that *Gynura procumbens* extract administration can augment VEGF expression, expedite angiogenesis and rehabilitate the architecture of skin tissue affected by diabetic wounds. Moreover, it asserts that one of the active phytochemicals in the extract demonstrates a strong binding affinity to VEGF, hence potentially stabilizing the VEGF structure compromised by oxidative stress in diabetic situations.

MATERIALS AND METHODS

Study area: This study was conducted at the Animal House Laboratory and the Laboratory of Animal Physiology, Department of Biology, Faculty of Mathematics and Natural Sciences, Universitas Sumatera Utara, Medan, North Sumatra, Indonesia. All experimental procedures, including animal induction, treatment, sample collection and immunohistochemical analysis, were performed from January, 2025 to September, 2025.

Chemicals and reagents: The reagents used for the immunohistochemistry: Invitrogen VEGF Polyclonal Antibody (Cat # PA5-85171,100 µL) from ThermoFisher Scientific, USA. Furthermore, a phosphate-buffered saline (PBS) solution was employed, which consisted of a 50% glycerol and 1% bovine albumin (BSA) buffer (Catalogue Number BS-0812R).

Preparation of the *Gynura procumbens* (GB) leaves: The 70% ethanol extract of *Gynura procumbens* was acquired by the maceration method. Fresh *Gynura procumbens* leaves were thoroughly washed, air-dried to reduce moisture content and subsequently ground into a coarse powder. One hundred grams of powder was macerated in a 70% ethanol solvent at a 1:10 (w/v) ratio for 72 hours at room temperature, with periodic agitation to improve extraction efficiency. The solution was subsequently filtered via filter paper to separate the residue. The filtrate was subsequently evaporated using a rotary evaporator at 40-50°C until a viscous extract was obtained. The extract was stored in a sealed container and kept at 4°C until used for further investigation.

Analysis by Liquid Chromatography-Mass Spectrometry (LC-MS/MS): The phytochemical analysis of the ethanolic extract of *Gynura procumbens* was conducted using LC-MS/MS with an electrospray ionization (ESI) source functioning in both positive and negative ion modes. The chromatographic separation employed a reverse-phase C18 column with a gradient elution system including solvent A (water with 0.1% formic acid) and solvent B (acetonitrile with 0.1% formic acid). The flow rate was established at 0.3 mL/min, with a total duration of around 20 minutes. Mass spectrometry detection utilized a triple quadrupole mass analyzer, with the scanning range established between m/z 100 and 1000. Compounds were identified by comparing their exact mass, fragmentation pattern and retention time with reference spectra from literature and public sources, such as PubChem and MassBank. The chromatograms were examined to identify the primary ingredients according to peak intensity and the five most abundant compounds were chosen for further investigation of biological relevance and *in silico* docking to VEGF protein targets.

Data mining: The target protein, Vascular Endothelial Growth Factor (VEGF), was retrieved from the NCBI (National Center for Biotechnology Information) database using its accession number AAL07528 and downloaded in FASTA format for further structural modeling with AlphaFold. The ligand compounds were selected based on their pharmacological relevance, particularly their potential anti-angiogenic properties. Molecular structures of Alloxan (PubChem CID: 5781), Luteolin (CID: 5280445), Kaempferol 3-O-β-D-glucuronopyranoside (CID: 5318759), Trigonelline (CID: 5570) and Baicalin (CID: 64892) were downloaded from the PubChem database (https://pubchem.ncbi.nlm.nih.gov/) in 3D conformer formats (.sdf or.mol2) suitable for molecular docking. For Mahuannin F, the molecular structure was sourced from González-Juárez *et al.*,[20]. The compound was manually redrawn using ChemDraw and its 3D structure was optimized using Avogadro to generate a geometry suitable for computational analysis. All ligand structures were then converted and prepared in appropriate formats for subsequent molecular docking and dynamics simulations[21].

Molecular docking: Molecular docking was performed using CB-Dock2, a web-based protein-ligand docking tool that integrates AutoDock Vina with cavity detection and blind docking capability. The docking process aims to predict the binding affinity and interaction pose of selected ligands with the VEGF protein target. Before docking, the 3D structure of the VEGF protein (obtained via homology modeling or from PDB if available) was uploaded in PDB format to the CB-Dock2 server (http://cadd.labshare.cn/cb-dock2/). Each ligand, including Alloxan, Luteolin, Kaempferol 3-O-β-D-glucuronopyranoside, Trigonelline, Baicalin and Mahuannin F, was uploaded in .mol2 format, having been previously optimized in terms of geometry and energy minimization. CB-Dock2 automatically detects potential binding cavities in the protein structure and performs docking at multiple sites. The tool ranks the predicted binding modes based on AutoDock Vina binding scores (kcal/mol). For each ligand, the top-ranked binding pose with the most negative (i.e., lowest) binding energy was selected for further analysis. The docking results, including binding affinity values and ligand-protein interaction visualizations, were downloaded for interpretation. These included hydrogen bonding, hydrophobic contacts and π-π interactions observed within the predicted binding pockets. The docking outcomes were used to assess the relative binding strength and potential inhibitory effect of each compound on VEGF activity[22,23].

Molecular dynamics: Molecular dynamics (MD) simulations were performed using the CABS-flex 2.0 webserver (http://biocomp.chem.uw.edu.pl/CABSflex2) to assess the flexibility and structural stability of the target proteins. This platform utilizes a coarse-grained modeling approach with an implicit solvent environment, enabling efficient simulation of solvent effects without the need for explicit water molecules. The targets selected for MD analysis included native VEGF, VEGF in complex with Alloxan and VEGF-Alloxan further complexed with Mahuannin F. Simulations were executed using the default settings provided by CABS-flex, which comprise a simulation time equivalent to 10 nanoseconds, 50 monte carlo cycles and the generation of 50 trajectory frames per simulation. The system temperature was maintained at 300 K, mimicking

physiological conditions. Additionally, distance restraints were applied with a global weight of 1 to help preserve native-like contacts throughout the simulation. The root mean square fluctuation (RMSF) values obtained from these simulations offered valuable insights into the local flexibility and dynamic behavior of the protein and its complexes over the course of the simulation[22-25].

Animal handling: This study used 36 healthy male *Rattus norvegicus* Wistar strain rats weighing between 180 and 200 g. The rats had also reached sexual maturity at 11 and 14 weeks of age. Each group consisted of six male rats kept in each cage. The rats were acclimatized for 2 weeks in controlled laboratory conditions with a temperature of 25.3% c and a relative humidity of 35 to 60%. Throughout the day, the male rats were fed corn and pellets in an environment with constant lighting. They also had unlimited access to water. Acceptance of the study was granted by the Medical Research Ethics Committee of the Faculty of Mathematics and Natural Sciences, Medan, USU (reference number 0913/KEPH-FMIPA/2024).

Research design: Rats underwent overnight fasting before alloxan induction, excluding the standard treatment group (group A0). Alloxan was administered intraperitoneally at a dosage of 160 mg/kg of body weight on day 0. Three days later, blood glucose levels were assessed. Rats were classified as diabetic if their fasting blood glucose levels reached 200 mg/dl or above. The dorsal fur of the rat was removed and a lesion measuring 5 mm in diameter was produced using a punch biopsy tool. Anesthesia for wound creation began with the intramuscular injection of 0.2-0.3 mL of ketamine. The research included six groups. Group A0 served as a negative control to simulate standard conditions. A- consisted of alloxan-induced mice serving as a model for diabetic rats, whereas A+ encompassed alloxan-induced mice that were treated with bioplacenton ointment. A1 was induced with alloxan and administered GB leaves at a dose of 100 mg/kg body weight, whereas A2 was induced with alloxan and administered GB leaves at a dosage of 200 mg/kg body weight. A3 was administered alloxan and GB leaves at a dosage of 300 mg/kg of body weight. This herbal remedy is applied externally to treat ulcers in diabetic patients. Bioplacenton and *Gynura precumbens* (GB) ointment were administered for a period of 14 days. Ketamine injections were utilized for surgical purposes. The diabetic wound tissue was excised with surgical scissors for immunohistochemical examination.

Immunohistochemistry: Tissues were affixed to specialized glass slides using Menzel Superfrost Plus glue and air-dried overnight at 37°C for immunohistochemical examination. The objective lenses were coated with a coating of polylysine. The tissues were subjected to deparaffinization in xylene for two intervals of 15 minutes each, followed by gradual rehydration in alcohol solutions. The rehydration process entailed submerging the tissues in 96% ethanol for 2.5 minutes, followed by 70% ethanol for 2.5 minutes, with both stages executed twice[25]. The tissues were submerged for 15 minutes, thereafter rinsed with TBS buffer for 3 hours and 5 minutes. Thereafter, the tissues underwent dehydration through a sequence of ethanol solutions. Slides designated for VEGF staining were segregated and labeled to eliminate ambiguity. Antibody solutions were formulated with optimal dilutions. The antigen retrieval procedure is conducted at 105°C in a pressured steam apparatus called a decloaking chamber for 10-20 minutes, contingent upon the unique requirements and attributes of the antibody and tissue[26-28]. This phase seeks to enhance interaction between the antibody and the specific protein (antigen) in the tissue, hence reinforcing the antigen-antibody binding reaction. Rehydration is employed for antigen retrieval. The substance is subsequently heated in citrate buffer utilizing microwave radiation for five minutes. The sample is thereafter rinsed thrice for five minutes each using phosphate-buffered saline Tween 20 (PBST) solution[29]. The buffer for each antibody is meticulously formulated. A 3% Hydrogen Peroxide (H_2O_2) solution is employed to suppress endogenous peroxidase activity for 30 minutes. The sample is subsequently rinsed three times with phosphate-buffered saline Tween (PBST) for five minutes per rinse. To prevent nonspecific binding, the tissue was incubated with 1% fetal bovine serum (FBS) for 30 minutes, subsequently undergoing three washes with PBST, each lasting five minutes. The tissue was subjected to treatment with primary antibodies, specifically VEGFR polyclonal antibodies, on each designated slide. The slides were subsequently incubated overnight at 40°C[30]. Subsequent to incubation, the slides were subjected to three washes with PBST, each lasting five minutes. The tissue was incubated with a biotinylated universal link secondary antibody for 30 minutes post-wash, followed by three rinses of five minutes each with PBST. The tissue was incubated with streptavidin HRP for 30 minutes, followed by three successive washes with PBST, each lasting five minutes. The chromogen 3,3'-diaminobenzidine (DAB) was administered to the tissue and incubated for 15 seconds. Subsequent to the DAB application, the slides were submerged in distilled

water and subsequently stained with Mayer's hematoxylin for 25 seconds, leading to the development of a brown chromogenic band. The tissue was subsequently rinsed with distilled water and desiccated using alcohol solutions of escalating concentration. The tissue was subsequently treated with xylene to eliminate any residual pollutants. The skin tissue on the slides was subsequently mounted with Permount and overlaid with a coverslip.

Statistical analysis of data: Data are reported as mean and standard deviation. The Kruskal-Wallis test was employed for non-parametric data, whereas the Mann-Whitney test was utilized for subsequent analysis. A p-value of less than 0.05 was deemed significant. The testing procedure encompassed hypothesis formulation, data presentation, test statistic calculation and conclusion derivation.

RESULTS

Phytochemical profiling of *Gynura procumbens* by LC-MS/MS: The LC-MS/MS study of the ethanol extract of *Gynura procumbens* identified five principal chemicals with differing response intensities. The chemical exhibiting the highest reaction was luteolin (62,727), succeeded by kaempferol 3-O-β-D-glucuronopyranoside (54,013), trigonelline (14,151), mahuannin F (14,096) and baicalin (11,185). The variations in ionization intensities suggest that luteolin and kaempferol are the predominant constituents in the extract, whereas mahuannin F and baicalin are present in comparatively lesser quantities (Table 1). The prevalence of luteolin and kaempferol corresponds with prior findings of elevated flavonoid levels in *G. procumbens*, which significantly contribute to biological functions including antioxidant activity, anti-inflammatory effects and the stimulation of angiogenesis. Trigonelline, albeit less prevalent than the primary flavonoids, was identified with a comparatively strong response, indicating the extract's potential to enhance the metabolic condition of diabetic wounds. The presence of mahuannin F and baicalin, albeit at reduced concentrations, is noteworthy due to their documented robust interactions with VEGF in *in silico* investigations. This underscores that, despite their comparatively low intensity, their biological impact can be substantial. Consequently, our LC-MS/MS profile table verifies that *G. procumbens* comprises a mixture of secondary metabolites from the flavonoid, alkaloid and polyphenol categories, collectively facilitating wound healing activity via the VEGF pathway and tissue regeneration.

Molecular docking of bioactive compounds with VEGF: Molecular docking simulations were conducted to examine the interactions of bioactive substances with Vascular Endothelial Growth Factor (VEGF) in diabetes-mimicking conditions, utilizing the VEGF–Alloxan complex as a model receptor. Alloxan, a recognized diabetogenic agent, was employed to simulate oxidative stress-induced alterations in VEGF, serving as a surrogate for the pathological wound milieu characteristic of diabetes. Each chemical was individually docked to the changed VEGF structure, enabling the assessment of its binding orientation, residue interactions and potential impact on the stability of the protein-ligand connection amid pathogenic changes (Fig. 1). Alloxan demonstrated a moderate binding affinity of -4.6 kcal/mol and established three conventional hydrogen bonds with SER170, GLN179 and CYS169. A π-alkyl interaction with LYS174 was identified, indicating hydrophobic stabilization. These interactions define the shallow polar region of the VEGF surface that is altered in the disease-mimicking model. The bound state of Alloxan acts as a benchmark for analyzing other ligand interactions. Luteolin demonstrates a binding score of -6.0 kcal/mol when docked to the VEGF-Alloxan complex. Significantly, it engages with residues distinct from those associated with Alloxan, encompassing π-π stacking and π-cation interactions with TRP10, as well as hydrogen bonding with SER6. The spatial variations in the binding pockets of Luteolin and Alloxan indicate that it does not directly interact with or interfere with the altered region of Alloxan. Luteolin interacts with a remote surface location, perhaps altering VEGF function via allosteric mechanisms or by stabilizing an alternative conformational domain without directly competing with the pathogenic modifier. Conversely, Kaempferol 3-O-β-D-glucuronopyranoside demonstrates restricted alignment with the Alloxan-interacting domain. A docking score of -6.4 kcal/mol signifies hydrogen bond formation with SER163, GLN179 and TRP162, in addition to interactions with PRO181 and CYS166 through π-alkyl and carbon-hydrogen interactions. The presence of residues linked to Alloxan indicates that Kaempferol may engage with the altered area of VEGF, potentially reinforcing or augmenting the connections impaired by Alloxan. The glycosylated structure of the flavonoid probably enhances the binding surface area and interaction flexibility, enabling the molecule to engage with various polar and hydrophobic areas surrounding the pathogen binding site. Conversely, Trigonelline demonstrates a reduced binding affinity (-3.8 kcal/mol) and exhibits considerable overlap with the

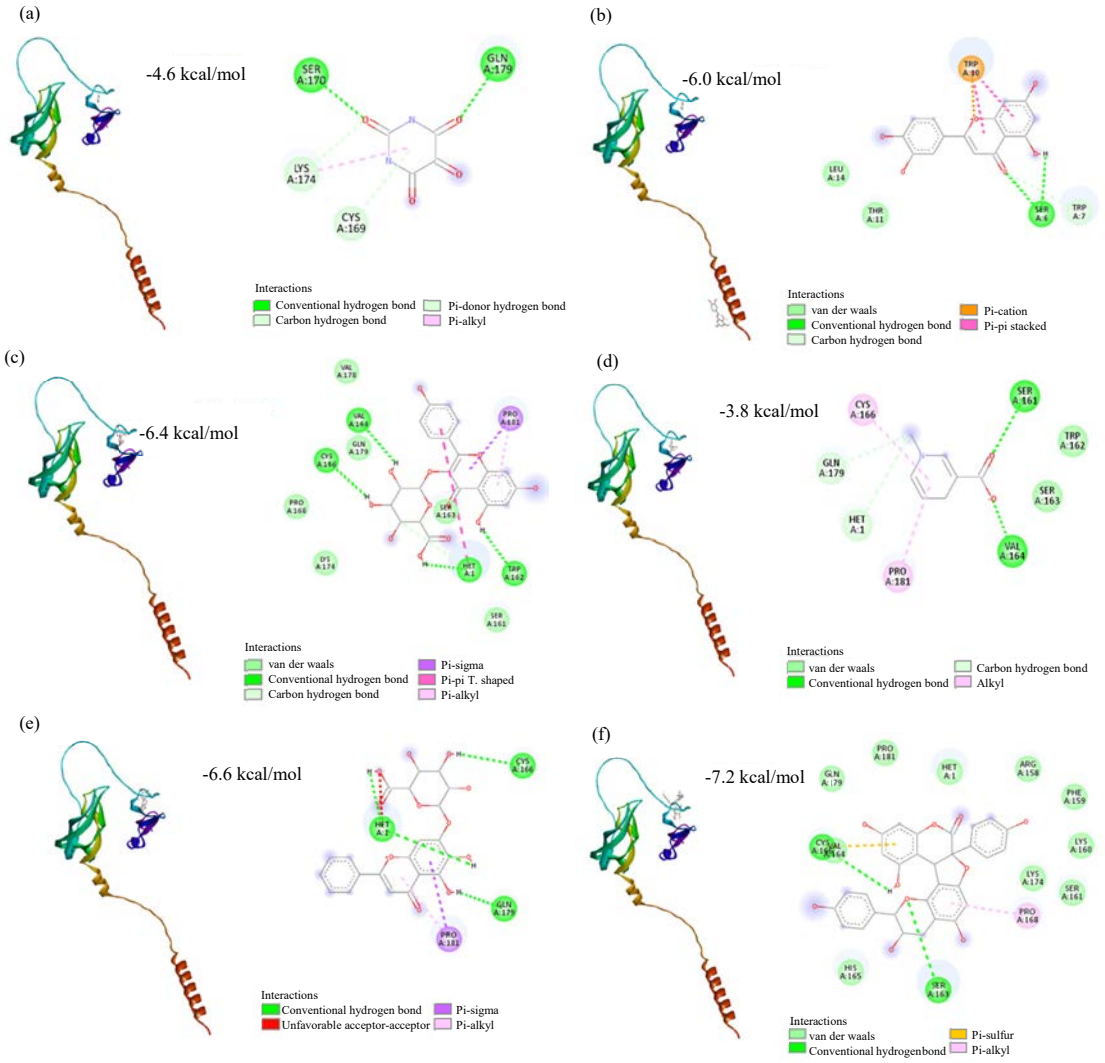

Fig. 1(a-f): Predicted binding interactions between VEGF and selected ligand combinations generated using CB-Dock2. The figure shows both the 3D binding conformations and 2D interaction diagrams of each complex. (a) VEGF+Alloxan (-4.6 kcal/mol), (b) VEGF+Alloxan+Luteolin (-6.0 kcal/mol), (c) VEGF+Alloxan+Kaempferol 3-O-β-D-glucuronopyranoside (-6.4 cal/mol), (d) VEGF+Alloxan+Trigonelline (-3.8 kcal/mol), (e) VEGF+Alloxan+Baicalin (-6.6 kcal/mol) and (f) VEGF+Alloxan+Mahuannin (-7.2 kcal/mol)

Table 1: Top 5 phytoconstituents from *Gynura procumbens* identified by LC-MS/MS analysis

No.	Compound name	Mode (ESI)	Response
1	Luteolin	ESI- and ESI+	62727
2	Kaempferol 3-O-β-D-glucuronopyranoside	ESI- and ESI+	54013
3	Trigonelline	ESI+	14151
4	Mahuannin F	ESI-	14096
5	Baicalin	ESI-	11185

Mode (ESI): Electrospray Ionization mode applied in LC-MS/MS analysis, consisting of ESI+ (positive ion mode) and ESI-(negative ion mode). Response: Peak intensity (signal response) indicating the relative abundance of each compound detected in the LC-MS/MS spectrum

Alloxan residue network, which includes SER161, SER163, GLN179, PRO181 and CYS166. Overlapping contacts indicate that Trigonelline directly competes with Alloxan for the same binding pocket, potentially resulting in steric hindrance or conformational stress in the VEGF-Alloxan complex. Instead of stabilizing the site, Trigonelline may intensify local interactions, indicating a potential antagonistic or destabilizing role within the diabetic VEGF framework.

Baicalin demonstrates an exceptional docking score of -6.6 kcal/mol and interacts with the residues CYS166, GLN179 and PRO181, which are similarly associated with Alloxan.

This overlapping interaction profile indicates that Baicalin targets the same modified area of VEGF, presumably in a structurally complementary fashion. Supplementary π-alkyl interactions and one adverse acceptor-acceptor interaction were noted; yet, the overall hydrogen bonding network seems to alleviate these destabilizing influences. Baicalin's interaction pattern indicates that this molecule may stabilize the conformational alterations induced by Alloxan through redundancy in polar contacts, potentially reinstating the partial integrity of the disrupted VEGF site. Among all the assessed compounds, Mahuannin F had the highest binding affinity at -7.2 kcal/mol. The extensive polyphenolic structure enables considerable hydrogen bonding with SER163, CYS164 and GLN179, along with π-sulfur and π-alkyl interactions with CYS164 and SER161. Supplementary van der Waals interactions with ARG158, LYS160 and PRO168 establish a dense interaction network. A multitude of residues are situated inside or adjacent to the Alloxan binding domain, indicating that Mahuannin F engages with analogous pathogen sites in a remarkably comparable fashion. The broad contact footprint indicates a considerable stabilizing influence on the modified VEGF surface, perhaps because of cooperative residue interactions and structural fortification. These findings underscore the distinct binding mechanisms and possible physiological functions of each medication in the context of diabetic VEGF malfunction. Compounds like Luteolin, which attach to specific spatial domains, may serve as allosteric regulators, whereas flavonoids such as Kaempferol and Baicalin demonstrate potential cooperative interactions with Alloxan-modified sites. Conversely, Trigonelline seems to impede Alloxan binding, potentially leading to increased instability. Mahuannin F is notable for its ability to establish a strong and stable interaction network, marked by high binding affinity and interactions with multiple essential residues linked to pathogen-binding sites. This capacity to establish a dense network of hydrogen bonds and hydrophobic contacts indicates a considerable degree of complementarity to the altered protein surface. After these findings, Mahuannin F was chosen for additional molecular dynamics simulations to examine the stability and conformational behavior of the VEGF-ligand complex over time, providing deeper insight into its potential therapeutic relevance in diabetic wound models.

Molecular dynamics simulation of VEGF complexes: The molecular dynamics visualization of Vascular Endothelial Growth Factor (VEGF) from *Rattus norvegicus* during a 10 nanosecond simulation demonstrates significant conformational alterations. At the outset (0–1 ns), the VEGF complex exhibits a compact, clustered configuration, likely signifying a bound or semi-bound docking state. Throughout the simulation (1-4 ns), a notable uncoiling and spatial reorganization of the helical domains transpires, particularly in the extended α-helix seen in purple and blue, indicating an initial structural adaptation phase to accommodate the bound ligand. A notable structural stability is observed at 5-6 nanoseconds. The protein adopts a bent yet structured conformation, suggesting a potential induced fit mechanism, in which VEGF undergoes structural modification to secure sustained interaction with its ligand. Significantly, within 6 to 10 nanoseconds, the VEGF molecule undergoes a partial reversion, followed by additional elongation and twisting of its helices. The rhythmic motion may indicate a dynamic binding interface characterized by transient interactions or flexible hinge regions that facilitate movement without diminishing overall ligand affinity (Fig. 2). The color-coded secondary structure elements (ranging from green to violet) maintain their relative integrity, suggesting that while global conformational changes occur, local secondary structures are preserved. The persistent helical extension and oscillation between compact and extended conformations suggest that VEGF in *Rattus norvegicus* may possess intrinsic flexibility crucial for receptor recognition or modulation of binding-induced signaling.

The VEGF from *Rattus norvegicus,* in combination with alloxan over a 10-nanosecond simulation, demonstrates significant and dynamic structural alterations relative to the VEGF-only system. At the initial time point (0-1 ns), the VEGF-alloxan complex begins in a somewhat compact shape. Unlike the VEGF-alone system, this complex exhibits more pronounced oscillations and prolonged compaction of the β-sheet regions (green and blue) throughout the simulation, suggesting a stabilizing impact due to alloxan binding. Within 2 to 5 ns, VEGF undergoes a progressive unwinding of the C-terminal α-helical tail (purple), whereas the core β-sheet domain remains compact and exhibits greater stability relative to the VEGF-only structure. The asymmetrical flexibility, marked by the dynamic variations of the helical section while the β-barrel core retains relative rigidity, suggests an alloxan-induced conformational locking at the ligand-binding interface (Fig. 3). The structural rigidity in the central region

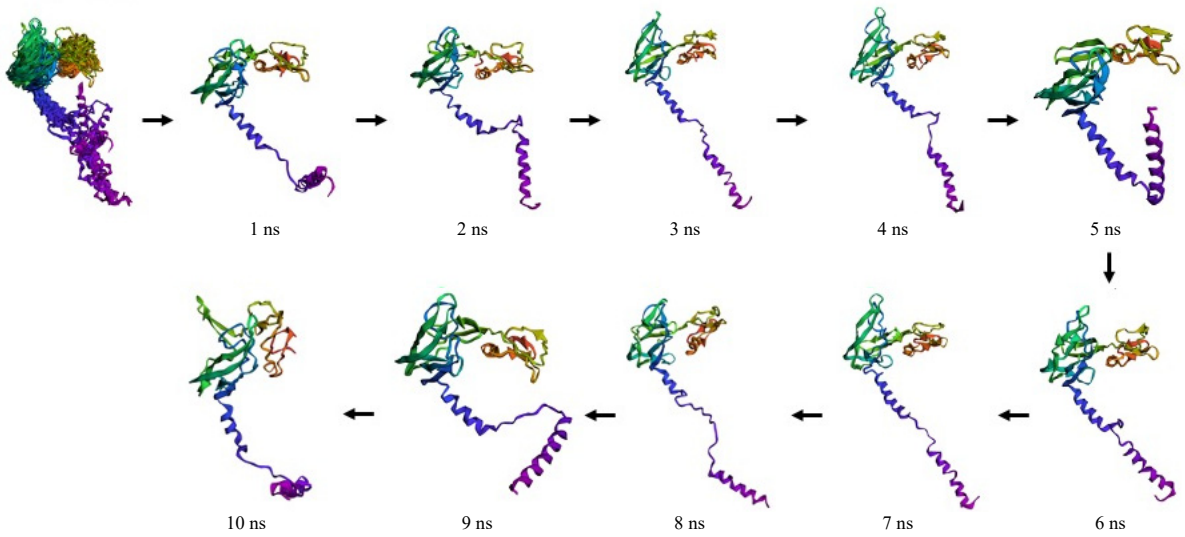

Fig. 2: Molecular dynamics simulation snapshots of VEGF from *Rattus norvegicus* native over a 10 ns timescale

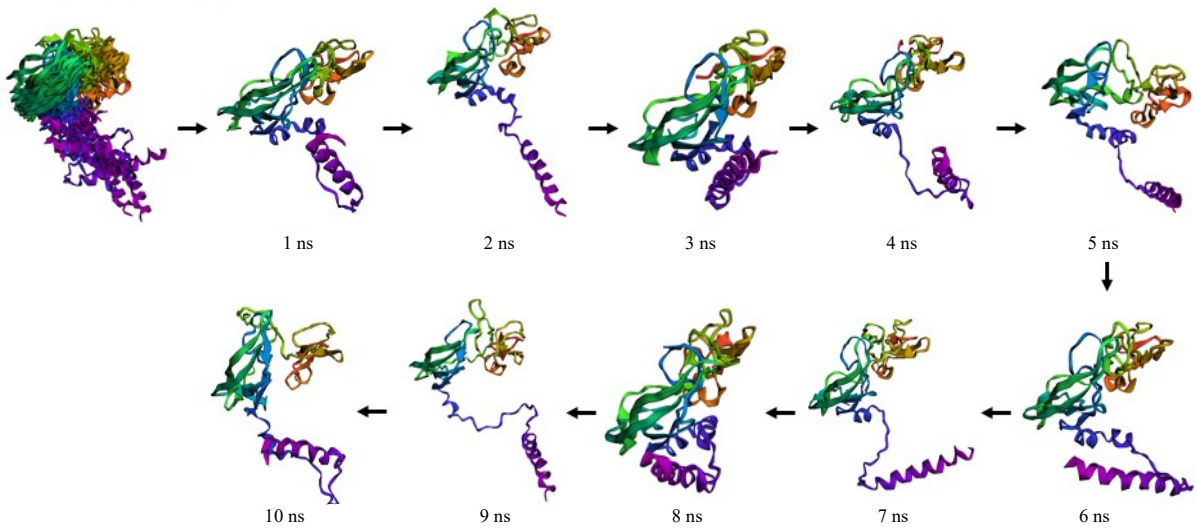

Fig. 3: Molecular dynamics simulation snapshots of VEGF from *Rattus norvegicus* in complex with alloxan over 10 ns, showing β-sheet compaction, C-terminal α-helix unwinding and ligand-induced structural rigidity

may impede VEGF's necessary flexibility for receptor binding and activation. Between 6 and 10 ns, the VEGF-alloxan complex exhibits repeated folding and coiling events, particularly within the extended helical domain, while preserving the integrity of the central β-sheet structure. These characteristics suggest that alloxan promotes localized motion restriction while permitting peripheral flexibility. This unique behavior signifies a partial inhibitory mechanism, whereby alloxan binding limits VEGF's functional flexibility by constraining domain rearrangements necessary for downstream signaling. Notably, unlike the VEGF-only system, the VEGF-alloxan combination demonstrates increased structural compactness and less conformational variability, especially inside the core domain. This may suggest a ligand-induced stabilizing action, hence reducing VEGF's bioactivity. The revised flexibility profile may be crucial for understanding how alloxan affects angiogenic signaling pathways through VEGF disruption, potentially contributing to its recognized diabetogenic effects via vascular regulation.

The VEGF protein from *Rattus norvegicus*, when complexed with alloxan and Mahuannin Fnin over a 10 nanosecond simulation, exhibits a distinctive pattern of conformational activity, indicating that Mahuannin Fnin stabilizes the structure against alloxan-induced disruption. Between 0 and 2 ns, the VEGF-alloxan-Mahuannin Fnin complex evolves from a compact conformation to a

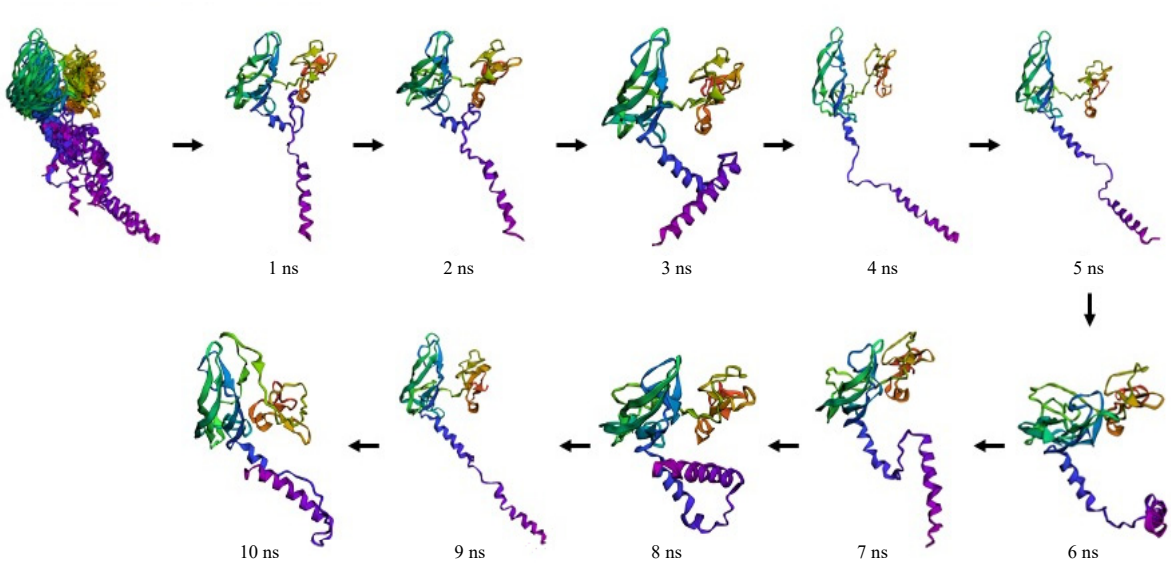

Fig. 4: Molecular dynamics simulation snapshots of VEGF from *Rattus norvegicus* in complex with alloxan and mahuannin fnin over 10 ns, illustrating stabilization of the β-sheet core and mitigation of alloxan-induced conformational changes

moderately stretched state, predominantly due to the uncoiling of the C-terminal α-helical region (depicted in purple). Notwithstanding this first rearrangement, the β-sheet-rich core (blue and green) maintains its integrity and does not experience the same extent of unfolding seen in the alloxan-only system. This preliminary stability suggests that Mahuannin Fnin may swiftly mitigate the conformational destabilization of VEGF caused by alloxan. A significant dynamic equilibrium manifests between 3 and 6 ns (Fig. 4). The VEGF backbone alternates between stretched and partially folded conformations, while circumventing the pronounced helical unraveling or misfolding observed in the alloxan-only complex. This is particularly evident in the frames at 4 ns and 6 ns, where the central β-sheets stay securely folded and the helices reorganize into structured secondary formations. This pattern indicates that Mahuannin Fnin may not strictly regulate VEGF but rather permits functional adaptability while mitigating excessive fluctuation. This aligns with the reduced median RMSF (1.80 Å) observed in quantitative analysis, where the majority of residues exhibited relative stability despite the presence of the destabilizing agent alloxan. A distinct event occurs between 7-10 ns, during which the helical tail exhibits a partial re-coiling maneuver, with residues refolding into a more compact and regular structure. This behavior significantly differs from the increasing disorder observed in the alloxan-only simulation and suggests a potential refolding process facilitated by Mahuannin Fnin. The compact shape achieved at 10 ns resembles the original VEGF state, suggesting a partial restoration of structural integrity, which may be crucial for maintaining biological functions such as receptor binding or angiogenic signaling. This image substantiates the idea that Mahuannin Fnin plays a preventive or restorative role, alleviating the detrimental effects of alloxan on VEGF conformation. By maintaining the integrity of the core structure and adjusting the flexibility of terminal areas, Mahuannin Fnin may stabilize VEGF in a manner more favorable to its physiological function. The findings, alongside RMSF data, robustly endorse the hypothesis that Mahuannin Fnin functions as a structural stabilizer under oxidative or glycotoxic stress, potentially possessing therapeutic significance in vascular complications related to diabetes or endothelial dysfunction.

Root mean square fluctuation (RMSF) analysis of VEGF complexes: An analysis of Root Mean Square Fluctuation (RMSF) was performed to assess the flexibility and dynamic behavior of each residue in the *Rattus norvegicus* VEGF protein under three distinct conditions: Native VEGF (control), VEGF complexed with alloxan (negative control) and VEGF complexed with both alloxan and the test compound Mahuannin F. The RMSF values provide quantitative insights into local residue mobility, directly reflecting the stability and structural integrity of the protein during the molecular dynamics simulation. The original VEGF structure had RMSF values ranging from 0.14 Å to 7.75 Å, with a mean variation of 2.31 Å and a median of 1.85 Å. The low RMSF values seen in most residues indicate a very stable protein structure, which

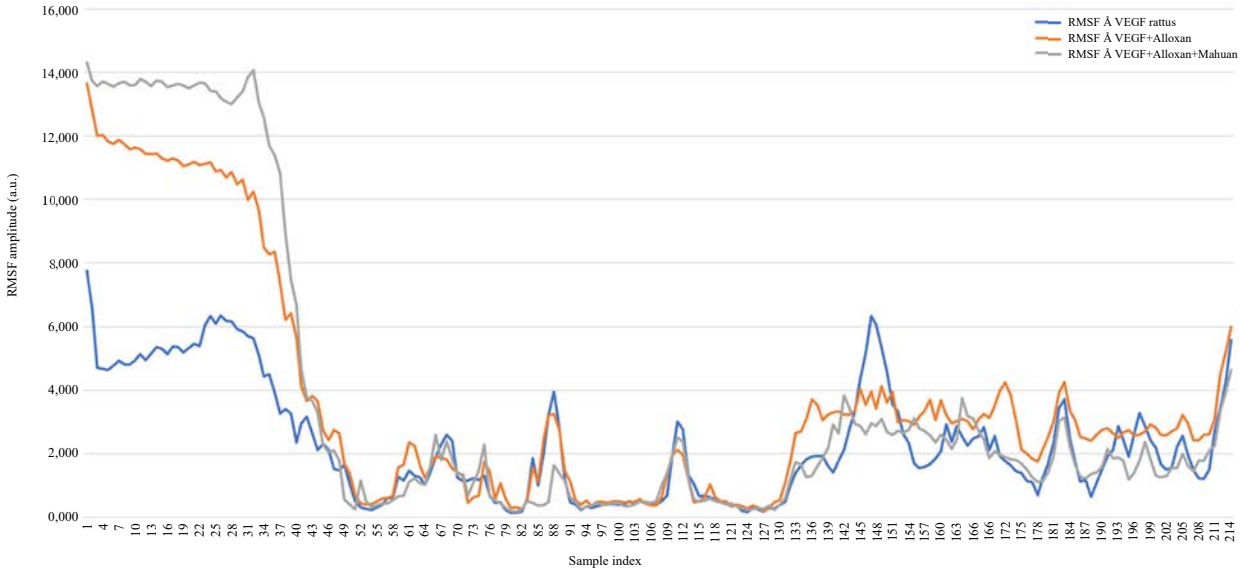

Fig. 5: Root Mean Square Fluctuation (RMSF) profiles over time in rats administered *Gynura procumbens* extract alone, with Alloxan and in combination with Mahuannin

is expected for a functionally effective VEGF capable of interacting with its receptor. The constrained mobility, particularly in the central β-sheet regions (residues ~100-150), underscores the presence of a structurally rigid core that is preserved throughout the simulation. Significantly, only a limited number of residues around the termini demonstrated increased flexibility, a typical characteristic resulting from their intrinsic solvent exposure and diminished secondary structural restrictions. Upon alloxan binding, a significant increase in residue flexibility was observed, with RMSF values rising to a maximum of 13.65 Å and a mean value of 3.68 Å. This sharp elevation in dynamic fluctuations, particularly pronounced at both the N- and C-terminal regions, suggests that alloxan binding induces conformational strain or destabilization within VEGF. The increased standard deviation of 3.59 Å, compared to 1.81 Å in the native form, reflects a broad distribution of residue mobility, further supporting the hypothesis that alloxan perturbs the native folding landscape of VEGF. These structural fluctuations may impair VEGF's ability to maintain a competent binding orientation or engage in downstream angiogenic signaling, consistent with its role as a known diabetogenic and vasculotoxic agent. Interestingly, co-administration of Mahuannin F with alloxan appears to partially attenuate this destabilizing effect. Although the greatest RMSF attains 14.32 Å, the mean RMSF persists at 3.67 Å, comparable to the alloxan-only group. The median RMSF decreases to 1.80 Å, signifying that a considerable number of residues exhibited decreased flexibility in the presence of Mahuannin F. This impact is most prominent in various loop regions and helices adjacent to the binding pocket, where alloxan-induced oscillations were previously most significant. The elevated standard deviation (4.61 Å) indicates that although Mahuannin F may not consistently diminish variations across all residues, it may provide localized stabilizing effects, particularly in structurally sensitive regions.

These tendencies are additionally corroborated by molecular dynamics trajectory visualizations. In the native VEGF simulation, the helical and β-sheet domains exhibit a stable orientation with just slight fluctuations at the termini. Conversely, the VEGF-alloxan complex experiences extensive structural alterations, characterized by notable twisting and loosening of the α-helical tail and disarray of peripheral loops. The introduction of Mahuannin F mitigates certain conformational instabilities; the helices exhibit a more consistent coiling pattern and the central β-sheet core remains more preserved, indicating the partial restoration implied by the RMSF profile. Collectively, these data indicate that alloxan compromises the structural integrity of VEGF by enhancing global residue mobility, potentially correlating with its pathogenic effects on angiogenesis. The incorporation of Mahuannin F alleviates certain effects by diminishing localized fluctuations and partially stabilizing the protein structure. This indicates that Mahuannin F may function as a structural modulator or protective agent against alloxan-induced injury, necessitating further exploration of its potential therapeutic significance in vascular health or diabetes consequences.

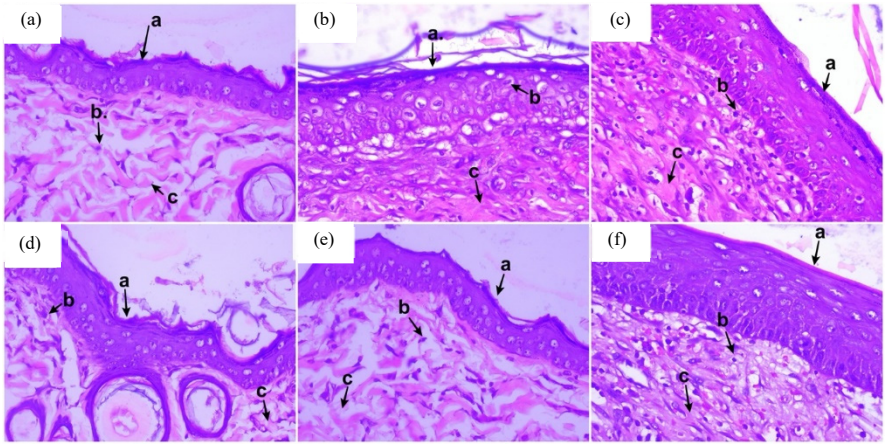

Fig. 6(a-f): Effect of *Gynura precumbens* on wound healing, (a) A0: Untreated rats, (b) A-: Only induced by alloxan, (c) A+: Induced by alloxan+pleasanton ointment, (d) A1: Induced by alloxan GB leaves at a dose of 100 mg/kg BW, (e) A2: Induced by alloxan GB leaves at a dose of 200 mg/kg BW and (f) A3: Induced by alloxan GB leaves at a dose of 300 mg/kg BW

a: Epithelium (topmost layer), b: Fibroblast cells (dark, oval nuclei in the dermis) and c: Collagen fibers (pink/red areas with fibers) (400x)

Table 2: Analysis of tissue from diabetic wounds using Hematoxylin and Eosin staining

Treatment	Epithelial tissue thickness (μm)	Number of fibroblast cells	Collagen
A0	33.26±4.31^{a}	70.19±7.59^{a}	1.45±0.17^{a}
A-	26.28±5.23^{b}	76.28±6.33^{b}	2.41±0.16^{b}
A+	49.52±3.54^{b}	64.21±6.19^{a}	2.45±0.09^{ab}
A1	30.18±4.83^{b}	74.25±7.30^{b}	2.75±0.10^{bc}
A2	35.32±3.28^{bc}	65.42±8.107^{b}	2.95±0.1^{c}
A3	47.36±4.27^{c}	64.15±8.62^{a}	3.52±0.08^{d}

A0: Untreated rats, A-: Only induced by alloxan, A+: induced by alloxan+Pleasanton ointment, A1: Induced by alloxan GB leaves at a dose of 100 mg/kg BW, A2: Induced by alloxan GB leaves at a dose of 200 mg/kg BW, A3: Induced by alloxan GB leaves at a dose of 300 mg/kg BW. Values are expressed as Mean±SD (n = 36), Statistical analysis was performed using One-way ANOVA followed by Duncan's *post hoc* test (different notations indicate significant differences)

Histological analysis of diabetic wound healing (H&E staining): The thickness of epithelial tissue can influence the extent of tissue injury. The minimal epithelial thickness was seen in the diabetic rat group as indicated in Table 2, where diabetes wounds inflict damage on the superficial tissue structure or epithelium, potentially disrupting the underlying tissue (Fig. 6). Histological analysis of diabetic wound tissues stained with hematoxylin and eosin (H&E) revealed distinct morphological variations among the experimental groups (Fig. 6a-f). The untreated diabetic group (Fig. 6a) exhibited a thin and disorganized epithelial layer (a), extensive inflammatory cell infiltration (b) and disrupted collagen fibers (c), indicating impaired wound repair. In contrast, the alloxan-induced diabetic group receiving Bioplacenton ointment (Fig. 6b) demonstrated partial re-epithelialization with moderate fibroblast proliferation and beginning collagen organization, reflecting an initial phase of tissue recovery.

The group treated with a low concentration of *Gynura procumbens* extract (Fig. 6c) showed improved epithelial regeneration (a) and a noticeable increase in fibroblast number (b), although collagen deposition (c) remained loosely arranged. Further enhancement was observed in the medium-dose group (Fig. 6d), where epithelial continuity and fibroblast distribution were more organized compared to the low-dose group. The group treated with a high concentration of *Gynura procumbens* (300 mg/kg BW) (Fig. 6e) displayed a well-formed epidermal layer (a), denser fibroblast distribution (b) and compact collagen deposition (c), comparable to normal tissue architecture. Meanwhile, the combination group treated with *Gynura procumbens* and Bioplacenton ointment (Fig. 6f) exhibited the most balanced fibroblast proliferation and collagen density, closely resembling the normal skin structure. Collectively, these results indicate that increasing the dosage of *Gynura procumbens* correlates with improved epithelial regeneration, reduced inflammation and enhanced collagen organization. Fibroblasts, which play a pivotal role in collagen synthesis and the proliferative phase of wound healing, were optimally regulated in the high-dose *Gynura procumbens* group and the Bioplacenton-treated group. This finding suggests that *Gynura procumbens* exerts a wound-healing effect comparable to commercial Bioplacenton ointment in diabetic rat models (Fig. 6).

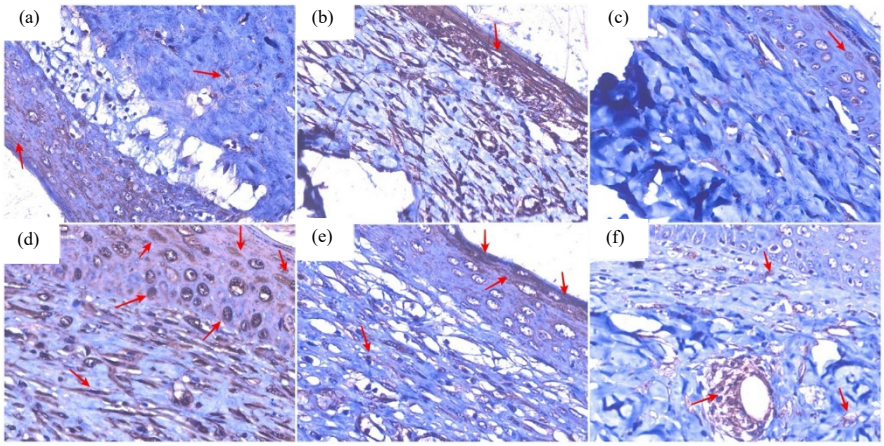

Fig. 7(a-f): Histological changes via VEGF in diabetic wounds after *Gynura precumbens* administration, (a) Untreated rats (A0), (b) Only induced by alloxan (A-), (c) Induced by alloxan+pleasanton ointment (A+), (d) Induced by alloxan GB leaves at a dose of 100 mg/kg BW (A1), (e) Induced by alloxan GB leaves at a dose of 200 mg/kg BW (A2) and (f) Induced by alloxan GB leaves at a dose of 300 mg/kg BW (A3)

The red arrow indicates positive VEGF expression (400x)

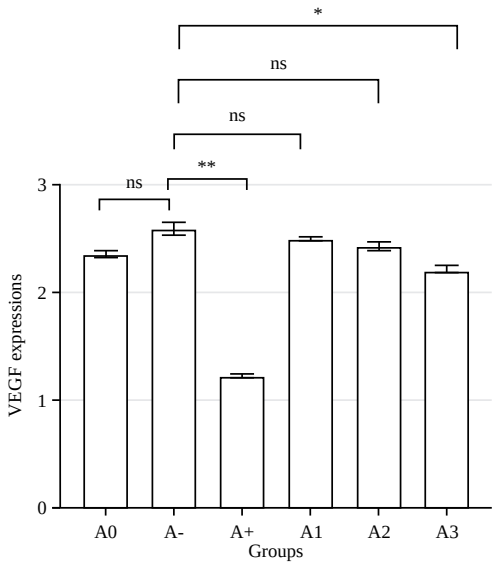

Fig. 8: Score of VEGF expression in diabetic wounds after administration of *Gynura precumbens.* A0: Untreated rats, A-: Only induced by alloxan, A+: Induced by alloxan+pleasanton ointment. A1: Induced by alloxan GB leaves at a dose of 100 mg/kg BW, A2: Induced by alloxan GB leaves at a dose of 200 mg/kg BW and A3: Induced by alloxan GB leaves at a dose of 300 mg/kg BW

Values are expressed as Mean±SD (n = 36), Statistical analysis was performed using Kruskal-Wallis followed by Mann-Whitney's *post hoc* test (*$p<0.05$ vs A-, **$p<0.01$ vs A-, $^{ns}p>0.05$)

Immunohistochemical analysis of VEGF expression: Immunohistochemical analysis of VEGF expression revealed distinct staining intensities among the experimental groups (Fig. 7a-f). The untreated diabetic control group (Fig. 7a) exhibited weak VEGF immunoreactivity, indicated by limited brown staining throughout the epidermal and dermal layers, reflecting impaired angiogenic signaling. Conversely, the diabetic group treated with Bioplacenton ointment (Fig. 7b) demonstrated minimal VEGF expression, suggesting reduced neovascular activity as healing progressed. The low-dose *Gynura procumbens* extract group (Fig. 7c) presented mild VEGF expression with localized staining, indicating the initiation of angiogenic responses. In the medium-dose group (Fig. 7d), VEGF labeling became more pronounced, particularly around proliferating fibroblasts and newly formed vasculature, suggesting enhanced tissue remodeling.

The high-dose *Gynura procumbens* group (Fig. 7e) displayed strong VEGF expression, corresponding to accelerated fibroblast proliferation, epithelial migration and collagen synthesis. The combination therapy group (Fig. 7f) showed the highest VEGF expression intensity, with dense, widespread staining in both epidermal and dermal regions, indicating optimized angiogenesis and extracellular matrix remodeling. These results demonstrate that increasing concentrations of *Gynura procumbens* positively regulate VEGF expression in diabetic wound tissue, promoting fibroblast activity, endothelial cell migration and structural restoration comparable to Bioplacenton ointment. This modulation of VEGF supports its mechanistic involvement in fibrosis and effective wound healing.

Quantitative analysis of VEGF expression demonstrated distinct differences among treatment groups (Fig. 8). The untreated control (A0) presented a moderate baseline level of VEGF, whereas the alloxan-induced diabetic group (A-) exhibited a slight increase, although the difference was not statistically significant (ns), indicating an early angiogenic response to hyperglycemic injury.

In contrast, diabetic rats treated with Bioplacenton ointment (A+) showed the lowest VEGF expression, which was significantly reduced compared to the A- group ($p<0.01$). This reduction suggests a more advanced healing phase characterized by declining angiogenic activity as tissue regeneration progresses. Rats treated with *Gynura procumbens* at 100 mg/kg BW (A1) and 200 mg/kg BW (A2) exhibited VEGF levels comparable to the control and diabetic groups (ns), indicating moderate angiogenic stimulation. Notably, the highest dose of *Gynura procumbens* (A3; 300 mg/kg BW) resulted in a significant increase in VEGF expression compared to Bioplacenton-treated rats ($p<0.05$), suggesting enhanced fibroblast proliferation, endothelial cell migration and extracellular matrix remodeling at this dosage.

Collectively, these findings indicate that *Gynura procumbens* modulates VEGF in a dose-dependent manner, with the highest concentration promoting optimal angiogenesis in diabetic wounds, consistent with improved histological tissue architecture observed in immunohistochemical analysis. These results further support the role of phytochemical components in regulating growth factor-mediated wound healing dynamics.

DISCUSSION

The wound healing process in diabetic patients is significantly hampered by chronic hyperglycemia, which causes oxidative stress, impaired immune response and decreased angiogenesis[31]. Hematoxylin and Eosin (H&E) staining of skin tissue revealed substantial morphological discrepancies among treatment groups. Group A0 (normal) exhibited a preserved epithelial architecture with uniform thickness and equitable fibroblast dispersion, indicative of healthy tissue conditions. Conversely, group A- (diabetes without treatment) had reduced epithelial thickness, tissue disarray and a compensatory rise in fibroblast count, indicative of the inflammatory response to diabetic wounds. Group A+ (bioplacenton) demonstrated a notable enhancement in epithelial structure, characterized by enhanced epithelial thickness, albeit with a reduction in fibroblast count, potentially attributable to the topical healing effect that expedites the remodeling process. Groups A1 and A2 (at doses of 100 and 200 mg/kg *Gynura procumbens*) exhibited a gradual augmentation in epithelial thickness, a balanced count of fibroblasts and heightened collagen density, signifying a progressive regenerative response. Conversely, group A3 (300 mg/kg dose) had nearly normal epithelial thickness, an ideal fibroblast count and the maximum collagen density, signifying a wound healing process most like to healthy tissue and demonstrating the greatest efficacy of *Gynura procumbens* at that dosage[32].

This work illustrates that the topical application of *Gynura procumbens* (GB) can influence the wound healing process via molecular pathways that enhance Vascular Endothelial Growth Factor (VEGF) expression, augment collagen density and regulate fibroblast populations. Histological investigation revealed augmented epithelium thickness and collagen content in the group administered the maximum dosage of GB (300 mg/kg BW), comparable to the group treated with Bioplacenton ointment. In group A-, the epithelial tissue exhibited a thin appearance, uneven layering and minimal VEGF expression, indicating compromised angiogenesis and tissue regeneration. Group A+ (administered bioplacenton) exhibited enhanced epithelial structure, although it continued to demonstrate modest VEGF levels, suggesting a healing mechanism that does not entirely depend on the activation of the angiogenic pathway. In groups A1 and A2 (doses of 100 and 200 mg/kg), the epithelial architecture began to ameliorate and VEGF expression progressively increased, signifying the preliminary activation of the vascularization pathway[10]. Group A3 (300 mg/kg dosage) exhibited an epithelial architecture closely resembling normal tissue, with pronounced VEGF expression, demonstrating optimum angiogenesis activation that facilitates endothelial cell proliferation, fibroblast migration and collagen deposition. Consequently, the topical application of elevated dosages of *Gynura procumbens* has demonstrated the ability to restore tissue microarchitecture and enhance VEGF expression in the context of diabetic wound healing. This suggests that *Gynura procumbens*

functions as both an anti-inflammatory drug and a promoter of fibroblast proliferation and extracellular matrix deposition-two critical factors in the proliferative phase of wound healing[33,34]. Immunohistochemistry revealed a markedly elevated expression of VEGF in group A3 (300 mg/kg BW). The VEGF is crucial in angiogenesis and tissue regeneration by promoting endothelial cell migration and proliferation, along with collagen synthesis by fibroblasts. Elevated VEGF expression indicates that *Gynura procumbens* may enhance poor angiogenesis in diabetic wounds.

The results were supported by *in silico* methods employing molecular docking and molecular dynamics (MD) simulations. Mahuannin F, derived from GB extract, demonstrated the greatest binding affinity for VEGF (-7.2 kcal/mol) and engaged with critical residues in the alloxan-modified domain. The MD analysis demonstrated that the VEGF-Alloxan-Mahuannin F complex had enhanced structural stabilization relative to VEGF-Alloxan alone, as indicated by a reduction in the root mean square fluctuation (RMSF) at key residues. This indicates that Mahuannin F may safeguard VEGF from structural impairment caused by oxidative stress resulting from diabetes. Alongside Mahuannin F, drugs like Luteolin and Baicalin demonstrated sustained interactions with VEGF, either via competing processes at the same location or through allosteric modulation. Mahuannin F, although not demonstrating the highest intensity in LC-MS/MS data, was selected for comprehensive analysis in the *in silico* study because of its enhanced binding affinity to the VEGF target protein compared to the other four compounds. The docking score of Mahuannin F was -7.2 kcal/mol, which is lower (indicating stronger binding) than that of Luteolin, Kaempferol 3-O-β-D-glucuronopyranoside, Trigonelline and Baicalin. Mahuannin F established a comprehensive interaction network with essential residues in the alloxan-modified VEGF binding region, indicating a potential protective mechanism against protein dysfunction induced by oxidative stress in diabetic wounds. This finding was supported by molecular dynamics data demonstrating that the VEGF-Alloxan-Mahuannin F complex maintained conformational stability and shown decreased residue fluctuation compared to pathological conditions. Consequently, despite Mahuannin F's quantitative inferiority in the extract, its remarkable quality of structural and functional interactions makes it the most appealing option for further investigation into VEGF modulation and diabetic wound therapy[22,35].

The VEGF is essential for skin tissue regeneration in diabetic wounds by facilitating angiogenesis, the formation of new blood vessels required for supplying oxygen and nutrients to the wound area[36]. In diabetes, VEGF expression frequently declines due to oxidative stress and metabolic inefficiency, hence hindering tissue regeneration[10]. The treatment of *Gynura procumbens* markedly increases VEGF expression, especially at higher dosages (300 mg/kg BW), consequently augmenting vascularization, facilitating the migration and proliferation of endothelial cells and fibroblasts and boosting collagen synthesis by skin fibroblasts. The activation of VEGF accelerates re-epithelialization and strengthens the dermal structure, as seen by increased epithelial thickness and collagen density in the wound[37]. Thus, *Gynura procumbens* functions as a phytotherapeutic agent that stimulates VEGF synthesis and accelerates wound healing in the skin of diabetes patients. The findings of this study indicate that *Gynura procumbens* can augment VEGF expression and enhance the structural integrity of skin tissue in diabetic wounds; nevertheless, certain limitations should be recognized. This study did not evaluate the expression of other molecular pathways relevant to wound healing, including TGF-β, PDGF or inflammatory markers such as IL-1β and TNF-α, which could provide a more comprehensive knowledge of the herb's mechanism of action. Furthermore, *in silico* testing was restricted to a small selection of significant compounds, so the synergistic potential among phytoconstituents remained insufficiently explored. *in vivo* research was limited to a single animal model species with a topical focus and precluded other formulations, such as nanoemulsions, that could enhance skin penetration. Thus, the proposed follow-up involves the examination of nanoformulations derived from *Gynura procumbens,* thorough protein and genetic expression analysis via RT-PCR and western blot, along with initial clinical trials to evaluate its safety and efficacy in individuals as an adjunct therapy for diabetic wound healing.

CONCLUSION

The ethanol extract of *Gynura procumbens* markedly enhances diabetic wound healing by augmenting epithelial thickness, normalizing fibroblast counts, elevating collagen density and upregulating VEGF expression. The maximum dosage (300 mg/kg BW) exhibited the most significant restoration of skin architecture to that of normal tissue. *In silico* analysis verified that Mahuannin F, a principal phytoconstituent, demonstrates a robust binding affinity and stabilizing interaction with VEGF, safeguarding its structure from alloxan-induced disruption. These findings substantiate the therapeutic potential of *Gynura procumbens* in regulating angiogenesis and expediting wound repair under diabetic circumstances. Future research should investigate extensive molecular pathways, synergistic interactions of phytochemicals and clinical application via sophisticated formulations such as nanoemulsions.

SIGNIFICANCE STATEMENT

This study demonstrates that *Gynura procumbens* significantly promotes diabetic wound healing by enhancing VEGF expression, restoring epithelial thickness, normalizing fibroblast counts and increasing collagen density. The *in vivo* findings are supported by *in silico* evidence, where Mahuannin F showed the strongest binding affinity to VEGF and stabilized its structure against oxidative stress-induced disruption. These results highlight *G. procumbens* as a promising phytotherapeutic agent for accelerating angiogenesis and tissue regeneration in diabetic wounds, while also providing a molecular basis for the development of advanced formulations, such as nanoemulsions, for future clinical applications

ACKNOWLEDGMENT

This research was funded by the Ministry of Health, Indonesia, under Grant Number SP DIPA-024.12.2.632111/2025 dated December 2, 2024. The authors also acknowledge the support provided through the research award granted to Risma Dumiri Manurung, which contributed significantly to the successful completion of this study.

REFERENCES

1. Dasari, N., A. Jiang, A. Skochdopole, J. Chung, E.M. Reece, J. Vorstenbosch and S. Winocour, 2021. Updates in diabetic wound healing, inflammation, and scarring. Semin. Plast. Surg., 35: 153-158.
2. Spampinato, S.F., G.I. Caruso, R. de Pasquale, M.A. Sortino and S. Merlo, 2020. The treatment of impaired wound healing in diabetes: Looking among old drugs. Pharmaceuticals, Vol. 13. 10.3390/ph13040060.
3. Korkmaz, H.I., G. Flokstra, M. Waasdorp, A. Pijpe and S.G. Papendorp *et al*., 2023. The complexity of the post-burn immune response: An overview of the associated local and systemic complications. Cells, Vol. 12. 10.3390/cells12030345.
4. Aldekhayel, S., A.M. Khubrani, K.S. Alshaalan, M. Barajaa and O. Al-Meshal, 2021. Outcomes and complications of diabetic burn injuries: A single center experience. Int. J. Burns Trauma, 11: 220-225.
5. Papachristoforou, E., V. Lambadiari, E. Maratou and K. Makrilakis, 2020. Association of glycemic indices (hyperglycemia, glucose variability, and hypoglycemia) with oxidative stress and diabetic complications. J. Diabetes Res., Vol. 2020. 10.1155/2020/7489795.
6. Arya, A.K., R. Tripathi, S. Kumar and K. Tripathi, 2014. Recent advances on the association of apoptosis in chronic non healing diabetic wound. World J. Diabetes, 5: 756-762.
7. Riwaldt, S., T.J. Corydon, D. Pantalone, J. Sahana and P. Wise *et al*., 2021. Role of apoptosis in wound healing and apoptosis alterations in microgravity. Front. Bioeng. Biotechnol., Vol. 9. 10.3389/fbioe.2021.679650.
8. Zhang, G., P.N. Samarawickrama, L. Gui, Y. Ma and M. Cao *et al*., 2025. Revolutionizing diabetic foot ulcer care: The senotherapeutic approach. Aging Dis., 16: 946-970.
9. Rajendran, N.K., S.S.D. Kumar, N.N. Houreld and H. Abrahamse, 2019. Understanding the perspectives of forkhead transcription factors in delayed wound healing. J. Cell Commun. Signaling, 13: 151-162.
10. Johnson, K.E. and T.A. Wilgus, 2014. Vascular endothelial growth factor and angiogenesis in the regulation of cutaneous wound repair. Adv. Wound Care, 3: 647-661.
11. Veith, A.P., K. Henderson, A. Spencer, A.D. Sligar and A.B. Baker, 2019. Therapeutic strategies for enhancing angiogenesis in wound healing. Adv. Drug Delivery Rev., 146: 97-125.
12. Berlanga-Acosta, J., G.S. Schultz, E. López-Mola, G. Guillen-Nieto, M. García-Siverio and L. Herrera-Martínez, 2012. Glucose toxic effects on granulation tissue productive cells: The diabetics' impaired healing. BioMed Res. Int., Vol. 2013. 10.1155/2013/256043.
13. Tan, H.L., K.G. Chan, P. Pusparajah, L.H. Lee and B.H. Goh, 2016. *Gynura procumbens*: An overview of the biological activities. Front. Pharmacol., Vol. 7. 10.3389/fphar.2016.00052.
14. Tahsin, M.R., T.I. Tithi, S.R. Mim, Ehfazul Haque and A. Sultana *et al*., 2022. *In vivo* and *in silico* assessment of diabetes ameliorating potentiality and safety profile of *Gynura procumbens* leaves. Evidence-Based Complementary Altern. Med., Vol. 2022. 10.1155/2022/9095504.
15. Situmorang, P.C., W.F. Dewatisari, A. Setyawati, R.D. Manurung and E. Setiawan, 2025. Effect of *Gynura procumbens* (Lour.) Merr. on the histopathology of the diabetic pancreas via caspase family expression. J. Pharm. Pharmacogn. Res., 13: 836-847.
16. Cao, M.Y., J. Wu, L. Wu, Z. Gu, J.W. Hu, C.Q. Xie and W. Xiong, 2022. Anti-inflammatory effects of *Gynura procumbens* on RAW264.7 cells via regulation of the PI3K/Akt and MAPK signaling pathways. Evidence-Based Complementary Altern. Med., Vol. 2022. 10.1155/2022/5925626.
17. Kaewseejan, N., V. Sutthikhum and S. Siriamornpun, 2015. Potential of *Gynura procumbens* leaves as source of flavonoid-enriched fractions with enhanced antioxidant capacity. J. Funct. Foods, 12: 120-128.
18. Algariri, K., K.Y. Meng, I.J. Atangwho, M.Z. Asmawi, A. Sadikun, V. Murugaiyah and N. Ismai, 2013. Hypoglycemic and anti-hyperglycemic study of *Gynura procumbens* leaf extracts. Asian Pac. J. Trop. Biomed., 3: 358-366.
19. Situmorang, P.C., S. Wibowo, S. Ilyas, S.E. Nugraha and A.P. Nugraha *et al*., 2025. Therapeutic potential of *Gynura procumbens* in enhancing cytokine regulation in the cervix of rats induced by 7,12-dimethylbenz(a)anthracene: *In vivo* and *in silico* investigations. J. Funct. Foods, Vol. 132. 10.1016/j.jff.2025.106963.

20. González-Juárez, D.E., A. Escobedo-Moratilla, J. Flores, S. Hidalgo-Figueroa and N. Martínez-Tagüeña *et al*., 2020. A review of the *Ephedra* genus: Distribution, ecology, ethnobotany, phytochemistry and pharmacological properties. Molecules, Vol. 25. 10.3390/molecules25143283.
21. Wibowo, S., S.K. Wardhani, L. Hidayati, N. Wijayanti and K. Matsuo *et al*., 2024. Investigation of α-glucosidase and α-amylase inhibition for antidiabetic potential of agarwood (*Aquilaria malaccensis*) leaves extract. Biocatal. Agric. Biotechnol., Vol. 58. 10.1016/j.bcab.2024.103152.
22. Wibowo, S., S. Widyarti, A. Sabarudin, D.W. Soeatmadji and S.B. Sumitro, 2021. DFT and molecular dynamics studies of astaxanthin-metal ions (Cu^{2+} and Zn^{2+}) complex to prevent glycated human serum albumin from possible unfolding. Heliyon, Vol. 7. 10.1016/j.heliyon.2021.e06548.
23. Wibowo, S., J. Costa, M.C. Baratto, R. Pogni and S. Widyarti *et al*., 2022. Quantification and improvement of the dynamics of human serum albumin and glycated human serum albumin with astaxanthin/astaxanthin-metal ion complexes: Physico-chemical and computational approaches. Int. J. Mol. Sci., Vol. 23. 10.3390/ijms23094771.
24. Wibowo, S., S.B. Sumitro and S. Widyarti, 2020. Computational study of Cu^{2+}, Fe^{2+}, Fe^{3+}, Mn^{2+} and Mn^{3+} binding sites identification on HSA 4K2C. IOP Conf. Ser.: Mater. Sci. Eng., Vol. 833. 10.1088/1757-899X/833/1/012052.
25. Wibowo, S., S. Widyarti, A. Sabarudin, D.W. Soeatmadji and S.B. Sumitro 2019. The role of astaxanthin compared with metformin in preventing glycated human serum albumin from possible unfolding: A molecular dynamic study. Asian J. Pharm. Clin. Res., 12: 276-282.
26. Manurung, R.D., S. Ilyas, S. Hutahaean, R. Rosidah and P.C. Situmorang, 2022. Diabetic wound healing in IL-1β expression by nano herbal of *Zanthoxylum acanthopodium* and *Rhodomyrtus tomentosa*. Res. J. Pharm. Technol., 15: 2041-2046.
27. Manurun, R.D., S. Ilyas, S. Hutahaean, R. Rosidah and P.C. Situmorang, 2021. Diabetic wound healing in FGF expression by nano herbal of *Rhodomyrtus tomentosa* L. and *Zanthoxylum acanthopodium* fruits. Pak. J. Biol. Sci., 24: 401-408.
28. Wasnis, N.Z., S. Ilyas, S. Hutahaean, R. Silaban and P.C. Situmorang, 2022. Effect of *Vitis gracilis* wall (gagatan harimau) in the recovery of gastrocnemius muscle cells and cytochrome c expression of *Mus musculus*. J. Pharm. Pharmacogn. Res., 10: 303-309.
29. Situmorang, P.C., R.H. Simanullang, R.A. Syahputra, M.M. Hutahaean, H. Sembiring, L. Nisfa and E.R. Sari, 2023. Histological analysis of TGFβ1 and VEGFR expression in cervical carcinoma treated with *Rhodomyrtus tomentosa*. Pharmaciana, 70: 217-223.
30. Simanullang, R.H., P.C. Situmorang, M. Herlina, Noradina, B. Silalahi and S.S. Manurung, 2022. Histological changes of cervical tumours following *Zanthoxylum acanthopodium* DC treatment, and its impact on cytokine expression. Saudi J. Biol. Sci., 29: 2706-2718.
31. He, J., J. Chen, T. Liu, F. Qin and W. Wei, 2025. Research progress of multifunctional hydrogels in promoting wound healing of diabetes. Int. J. Nanomed., 20: 7549-7578.
32. Shita, A.D.P., A.W.S. Dharmayanti, Z. Meilawaty, M. Lestari and I.M.A. Mazaya, 2023. Increasing fibroblasts and gingival collagen density in periodontitis rats by using cassava leaf extract. J. Taibah Univ. Med. Sci., 18: 1321-1328.
33. Cialdai, F., C. Risaliti and M. Monici, 2022. Role of fibroblasts in wound healing and tissue remodeling on Earth and in space. Front. Bioeng. Biotechnol., Vol. 10. 10.3389/fbioe.2022.958381.
34. Sutthammikorn, N., V. Supajatura, H. Yue, M. Takahashi and S. Chansakaow *et al*., 2021. Topical *Gynura procumbens* as a novel therapeutic improves wound healing in diabetic mice. Plants, Vol. 10. 10.3390/plants10061122.
35. Zheng, S.Y., X.X. Wan, P.A. Kambey, Y. Luo and X.M. Hu *et al*., 2023. Therapeutic role of growth factors in treating diabetic wound. World J. Diabetes, 14: 364-395.
36. Huang, K., B. Mi, Y. Xiong, Z. Fu and W. Zhou *et al*., 2025. Angiogenesis during diabetic wound repair: From mechanism to therapy opportunity. Burns Trauma, Vol. 13. 10.1093/burnst/tkae052.
37. Bao, P., A. Kodra, B.A.M. Tomic-Canic, M.S. Golinko, H.P. Ehrlich and H. Brem, 2009. The role of vascular endothelial growth factor in wound healing. J. Surg. Res., 153: 347-358.